J Solid State Electrochem (2001) 5: 196–204
DOI 10.1007/s100080000138

ORIGINAL PAPER

Dina Fattakhova · Ladislav Kavan · Petr Krtil

Lithium insertion into titanium dioxide (anatase) electrodes: microstructure and electrolyte effects

Received: 5 March 1999 / Accepted: 7 April 2000 / Published online: 1 March 2001

Abstract Insertion characteristics of anatase electrodes were studied on single-crystal and polycrystalline electrodes of different microstructures. The lithium incorporation from propylene carbonate solution containing $LiClO_4$ and $Li(CF_3SO_2)_2N$ was studied by means of cyclic voltammetry (CV), the quartz crystal microbalance (QCM) and the galvanostatic intermittent titration technique (GITT). The electrode microstructure affects both the accessible coefficient x and the reversibility of the process. The highest insertion activity was observed for electrodes composed of crystals with characteristic dimensions of ~10^{-8} m. The insertion properties deteriorate for higher as well as for smaller crystal sizes. Enhanced insertion was observed in $Li(CF_3SO_2)_2N$-containing solutions. Lithium insertion is satisfactorily reversible for mesoscopic electrodes; the reversibility in the case of compact polycrystalline and single-crystal electrodes is poor. The reversibility of the insertion improves with increasing electrolyte concentration. The lithium diffusion coefficient decreases with increasing x and ranges between 10^{-15} and 10^{-18} cm^2 s^{-1}.

Key words Titanium dioxide · Anatase · Lithium insertion · Galvanostatic intermittent titration technique · Quartz crystal microbalance

Introduction

Interest in the electrochemistry of titanium dioxide has been triggered mainly by its possible application in, for example, 2 V lithium secondary batteries [1, 2, 3, 4, 5, 6] or in electrochromic devices [7, 8]. Although titanium dioxide exists in eight different crystallographic modifications [9], lithium insertion has been studied only for anatase and rutile [10, 11]. Anatase is generally considered to be the more active Li^+ insertion host; insertion into rutile is reported to be negligible [1, 2, 10, 12]. Nevertheless, recent investigations show that lithium insertion into rutile electrodes proceeds at potentials negative to 1.5 V (Li/0.5 M Li^+) [13].

Insertion of lithium into anatase was studied using various techniques with single-crystal as well as polycrystalline electrodes. Despite the attention paid to this process so far, there still remains some controversy. The diffusion coefficients for polycrystalline anatase exhibit a large spread between ca. 10^{-10} to 10^{-17} cm^2 s^{-1} [4, 8, 14, 15, 16]; disagreement also exists about the nature of the final insertion product [1, 2, 8, 17, 18]. Another work (which does not specify the crystallographic form of the studied TiO_2) concluded that Li^+ diffusion in TiO_2 is limited only to the accumulation layer of thickness about 11 nm [19]. This conflicts with a study of anatase single crystals, showing diffusion distances as large as 390 nm [20].

Another still open issue is the effect of the anatase electrode microstructure on the insertion activity. Besides the anatase single-crystal electrode, which was prepared and studied recently [20], there are several routines to prepare anatase polycrystalline electrodes with different microstructures [21, 22, 23]. In this paper we present the results of a comparative study of lithium insertion into anatase electrodes with different microstructures. Electrochemical and electrochemical quartz crystal microbalance (EQCM) data, measured on the anatase single-crystal and polycrystalline electrodes, prepared either by electrodeposition [21], spray pyrolysis [22] or by sintering of colloidal anatase particles [24], are used to show the influence of the electrode microstructure on the insertion behavior. Attention was paid mainly to the effect of the electrode microstructure on the accessible insertion capacity and charge and mass reversibility.

D. Fattakhova · L. Kavan · P. Krtil (✉)
J. Heyrovský Institute of Physical Chemistry,
Academy of Sciences of the Czech Republic,
Dolejškova 3, 182 23 Prague, Czech Republic
E-mail: krtilp@jh-inst.cas.cz

D. Fattakhova
Department of Physical Chemistry,
Kazan State University, Kazan, Russia

Experimental

Propylene carbonate (PC; Fluka) was vacuum distilled and dried over 4 Å molecular sieves before use. $LiClO_4$ and $Li(CF_3SO_2)_2N$ (both Fluka) were dried at 120 °C/0.1 mPa. All solutions were prepared and stored in an argon-filled glove box (O_2 and water content < 10 ppm); the electrolyte solutions were purged with argon and dried over molecular sieves. A typical trace water content was 9 ppm in $LiClO_4$ and 30 ppm in $Li(CF_3SO_2)_2N$-containing solutions as measured by Karl Fischer titration using the WTK 891 titrator (Diram, Czech Republic).

An anatase single crystal [orientation (101)], prepared by a chemical transport reaction [6] and doped in a hydrogen atmosphere at 500 °C, was used in the electrochemical experiments. Anatase polycrystalline electrodes were prepared as follows. Mesoscopic electrodes were made by sintering of TiO_2 colloid at 450 °C for 45 min [24, 25]. Compact polycrystalline films were made by spray pyrolysis of Ti(IV) di-iso-propoxy titamium bis(acetylacetonate) at 450 °C [22] and by anodic oxidation of $TiCl_3$ in acidic aqueous media with subsequent annealing of the deposit at 450 °C [21]. AT-cut 10 MHz quartz crystals (International Crystal Manufacturing Company, Okla., USA) with deposited "key-hole" shaped gold contacts (1000 Å Au on 100 Å of Cr) were used in QCM measurements as the mass sensing probes. Polycrystalline TiO_2 layers were deposited directly on gold crystal contacts; the projected area of the electrodes was the same as the piezoactive area of the crystals (i.e. 0.22 cm^2). The surface coverage of the mesoscopic films was generally in the range 40–100 μg cm^{-2}, which corresponds to a thickness range of 0.4–1.2 μm. The surface coverage of electrodeposited and spray pyrolysis prepared electrodes was below 10 μg cm^{-2}.

All electrochemical experiments were performed in a three-electrode arrangement with a Pt foil auxiliary electrode using the PAR 263A potentiostat. Working electrode potentials were measured and are quoted with respect to the Li/Li^+ reference electrode, as indicated in the figure captions. The mass change signals were measured using a QCM apparatus based on the circuitry described by Bruckenstein et al. [26].

Open circuit potential measurements were measured in the following way. The electrodes were first reduced (oxidized) by a galvanostatic step until a definite amount of charge passed through the system. Then the auxiliary electrode was disconnected and the open circuit potential recorded for 45 min. The galvanostatic charge injections were repeated until the total injected charge was equal to $x \approx 0.2$. Subsequently, the polarity of the controlled current was reversed and a set of oxidation steps was performed. The mode of the open circuit potential measurement complied with the galvanostatic intermittent titration technique (GITT) [27].

Results and discussion

The data characterizing the respective microstructures – typical crystal size and estimated roughness factor – of the electrodes employed in the study are summarized in Table 1. Particle size values of the polycrystalline electrodes shown in Table 1 were estimated from X-ray diffraction. The actual surface areas of polycrystalline electrodes used to calculate roughness factors ($S_{actual}/S_{projected}$) were calculated from the specific surface area (determined using the BET method) and the actual electrode mass. Scanning electron micrographs of the anatase electrode surfaces can be found elsewhere [23]. Corresponding cyclic voltammograms in propylene carbonate based solutions containing 0.5 M $Li(CF_3SO_2)_2N$ and $LiClO_4$ are plotted in Fig. 1.

Table 1 Particle size and roughness factors for various anatase electrodes

Electrode	Particle size (m)	Roughness factor
Single crystal	$\sim 10^{-3}$	~1
Electrodeposited	5×10^{-9}	1–2
Spray pyrolysis	5×10^{-8}	~10
Mesoscopic	1×10^{-8}	100–1000

Electrode potential

The insertion behavior of anatase electrodes is characterized by a current peak at ca. 1.6 V during the initial cathodic scan and by a current peak at ca. 2.0 V in the subsequent anodic scan [20, 23]. These peaks can be traced in voltammograms for all studied electrodes. Peaks are better pronounced in $Li(CF_3SO_2)_2N$-containing electrolytes (see dashed curves in Fig. 1). The stoichiometry of the insertion process is most often expressed as:

$$TiO_2(s) + xLi^+(l) + xe^- \rightarrow Li_xTiO_2(s) \quad (1)$$

The coefficient x is usually employed to compare the insertion performance of different electrodes. The formal potentials, estimated by averaging the peak potentials, are sensitive to a change of lithium concentration and show a nearly Nernstian response in the concentration range 0.05–2 M (see Fig. 2). On the other hand, the change of the electrolyte concentration has a much more complex effect on the currents. Peak currents increase with increasing electrolyte concentration for concentrations lower than 1 M. A tenfold increase of the Li^+ concentration in this region leads to a ca. 20% increase of the peak currents. For the concentration region above 1 M, the electrolyte increase leads to a smaller change of the peak current. Increase of electrolyte concentration, however, leads also to a change of the peak separation, which shows a minimum at a salt concentration of 1 M. This minimum of the peak separation tracks the maximum of the conductivity of the $Li(CF_3SO_2)_2N$/propylene carbonate system [28]. The change in the peak separation accompanying the change in peak currents indicates the uncompensated iR drop in the solution as the major reason for the peak current change. The iR effects are more significant in the case of $Li(CF_3SO_2)_2N$-containing solutions. Estimates of the standard potentials extracted from the voltammetric measurements on different electrodes are summarized in Table 2. As the data in Table 2 show, only the mesoscopic electrodes show reasonable agreement of the standard potential in both ClO_4^- and $(CF_3SO_2)_2N^-$ containing solutions. The values observed for all other electrode morphologies differ significantly in ClO_4^- and $(CF_3SO_2)_2N^-$ containing solutions (30–100 mV). Although one may expect a difference in electrode potentials due to different ion association in ClO_4^- and $(CF_3SO_2)_2N^-$ containing solutions, the observed differences cannot be assigned to

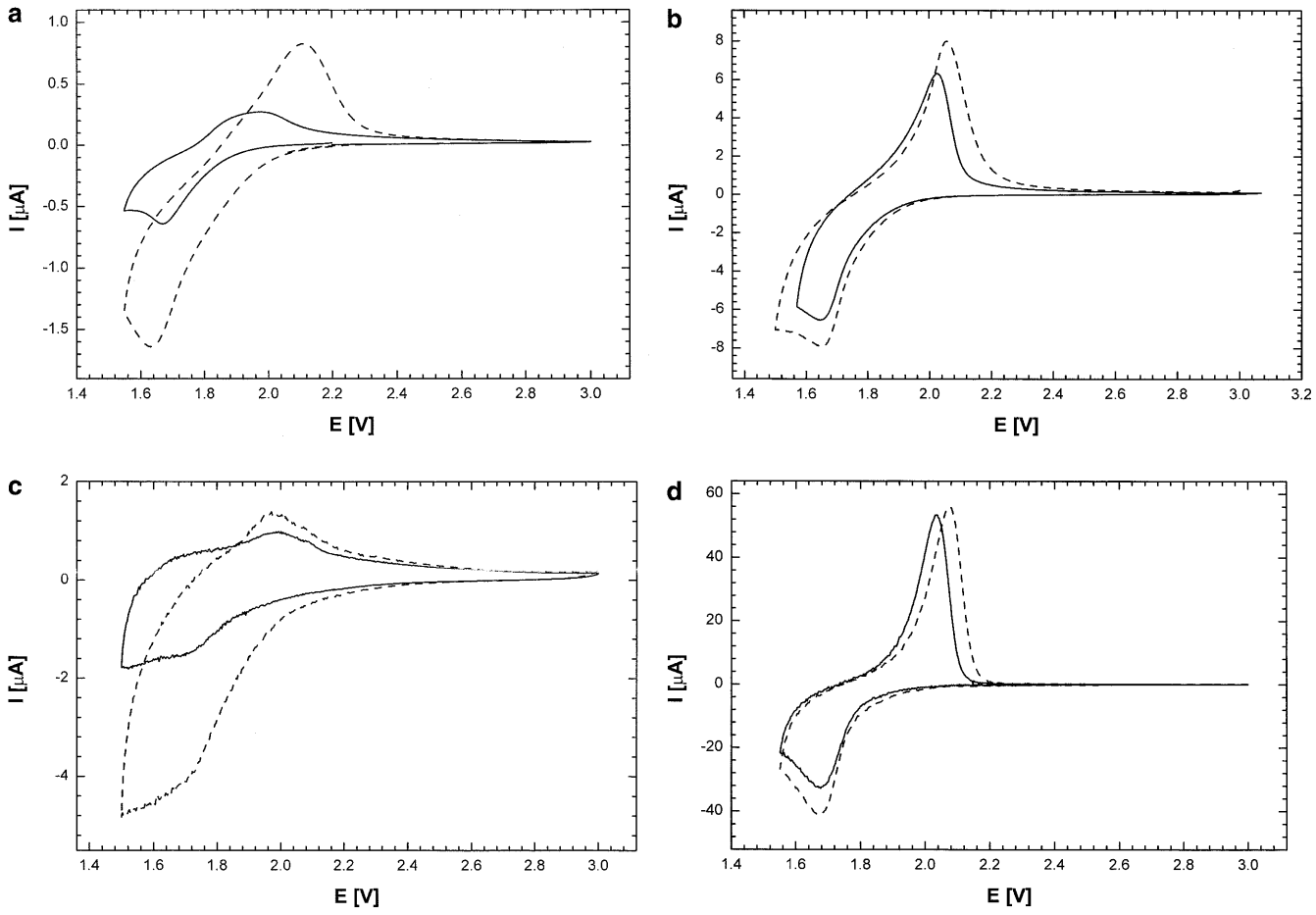

Fig. 1 Cyclic voltammograms of the anatase electrodes observed in 0.5 M $LiClO_4$/propylene carbonate (*solid line*) and 0.5 M $Li(CF_3SO_2)_2N$/propylene carbonate (*dashed line*) containing solutions: **a** single-crystal, **b** spray pyrolysis, **c** electrodeposited, **d** mesoscopic electrodes. Scan rate 2 mV s^{-1}; reference electrode Li/0.5 M Li^+

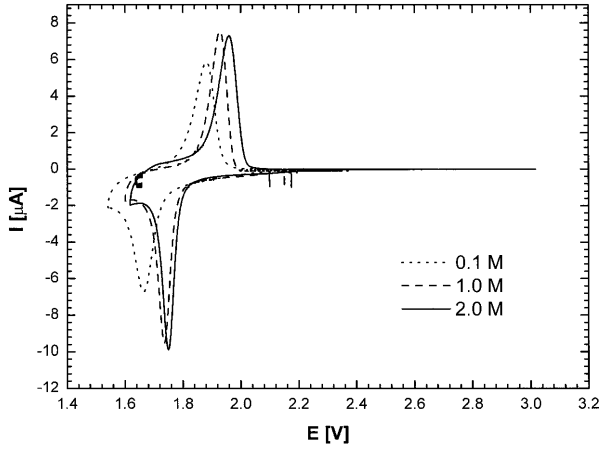

Fig. 2 Effect of the electrolyte concentration on the cyclic voltammograms of a mesoscopic anatase electrode in propylene carbonate-based solutions containing $Li(CF_3SO_2)_2N$. Concentration range 0.1–2.0 M. Reference electrode Li/1.0 M Li^+; scan rate 0.1 mV s^{-1}

such an effect. Certain deviations, however, may be expected by taking into account possible electrochemical side-reactions which can influence the potential reading via a mixed potential mechanism (vide infra).

While the response of the electrode potential to a change of the electrolyte concentration is Nernstian, the dependence of the electrode potential on the injected charge is, however, more complex (see Fig. 3). The open circuit potential (OCP) decreases with increasing x for values lower than 0.1. The OCP response to subsequent charge injection ($x > 0.1$) is different in 0.1 and 2 M solutions. In the 0.1 M solution, subsequent charge injection has no effect on the OCP. This may indicate a two-phase behavior. Such explanation is, however, opposed by the fact that subsequent oxidation can recover just about 40% of the injected charge. The significant discrepancy in the charge recovery can be explained by a relatively fast electrode self-discharge reaction. On the

Table 2 Estimates of the standard potential of electrodes with different morphologies

Electrode	0.5 M $LiClO_4$	0.5 M $Li(CF_3SO_2)_2N$
Single crystal	1.83	1.87
Electrodeposited	1.75	1.75
Spray pyrolysis	1.72	1.76
Mesoscopic	1.86	1.86

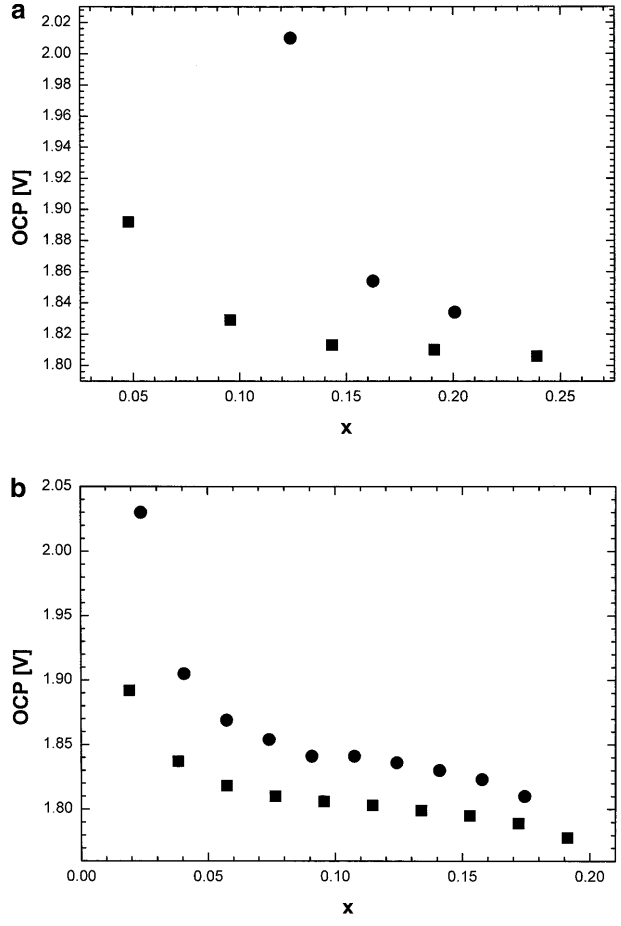

Fig. 3 Open circuit potential (OCP) vs. x dependence of a polycrystalline mesoscopic anatase electrode in **a** 0.1 M and **b** 2 M $Li(CF_3SO_2)_2N$/propylene carbonate solutions

other hand, in 2 M solution the OCP decreases with increasing x over the whole concentration range. Subsequent oxidation allows recovery of more than 90% of the injected charge, which indicates a much slower self-discharge rate in this concentration of the electrolyte. The final OCP values obtained during insertion steps were about 30 mV more negative than those observed at the end of corresponding oxidation steps. Therefore we can say that the observed final OCP values represent some quasi-equilibrium states rather than true thermodynamic equilibrium states.

The OCP data were used to calculate the lithium diffusion coefficient D as a function of x (see Fig. 4) according to the equation:

$$\tilde{D}_{Li} = \frac{4}{\tau\pi}\left(\frac{m_B V_m}{M_B S}\right)^2\left(\frac{\Delta E_s}{\Delta E_\tau}\right)^2 \quad (2)$$

where τ is the duration of the galvanostatic injection, m_B is the active electrode mass, M_B is molar mass of TiO_2, V_m is the molar volume, S is the actual electrode area, ΔE_s is the change of OCP value between two subsequent change injection steps and ΔE_τ is the total potential change during the galvanostatic charge injection.

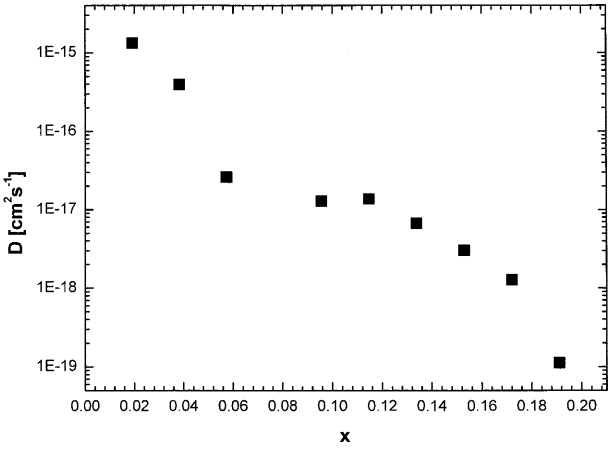

Fig. 4 Diffusion coefficient of Li in mesoscopic polycrystalline anatase as a function of coefficient x

The diffusion coefficient decreases with increasing x. The observed values of D range between 2×10^{-15} and ca. 1×10^{-18} cm^2 s^{-1}. The biggest change of D with coefficient x occurs below 0.05; above this value the increase in x has almost negligible effect on D. These data are 2–5 orders magnitude lower than those reported for anatase single crystals [20, 29]. On the other hand, they are in good agreement with data presented for similar electrodes in the literature [16].

Microstructure effects

The role of the electrode microstructure in the insertion process may be characterized in terms of, for example, average crystal size. The insertion activity can then be expressed using x, the charge reversibility Q_a/Q_c and the mass reversibility $\Delta m_a/\Delta m_c$.

Accessible insertion level and reversibility

The lithium insertion is a relatively slow process, i.e. we did not achieve a complete reduction of the electrodes on the time-scale corresponding to the polarization rate of 0.5 mV s^{-1}. The coefficients x extracted from cyclic voltammograms measured on different anatase electrodes are shown in Fig. 5. We did not observe x values higher than 0.5. The coefficients x observed in $Li(CF_3SO_2)_2N$-containing solutions were always higher than those obtained in $LiClO_4$-containing solutions.

The single-crystal electrode shows apparently the lowest insertion activity. The x values obtained for single-crystal electrodes were ca. 30 times lower than those for polycrystalline electrodes. The highest insertion response with x = ca. 0.45 was observed on mesoscopic electrodes with crystal size ~10 nm. The insertion activity of electrodes with a higher or lower characteristic crystal size was inferior to that of mesoscopic electrodes. In the case of single-crystal electrodes, the low values of

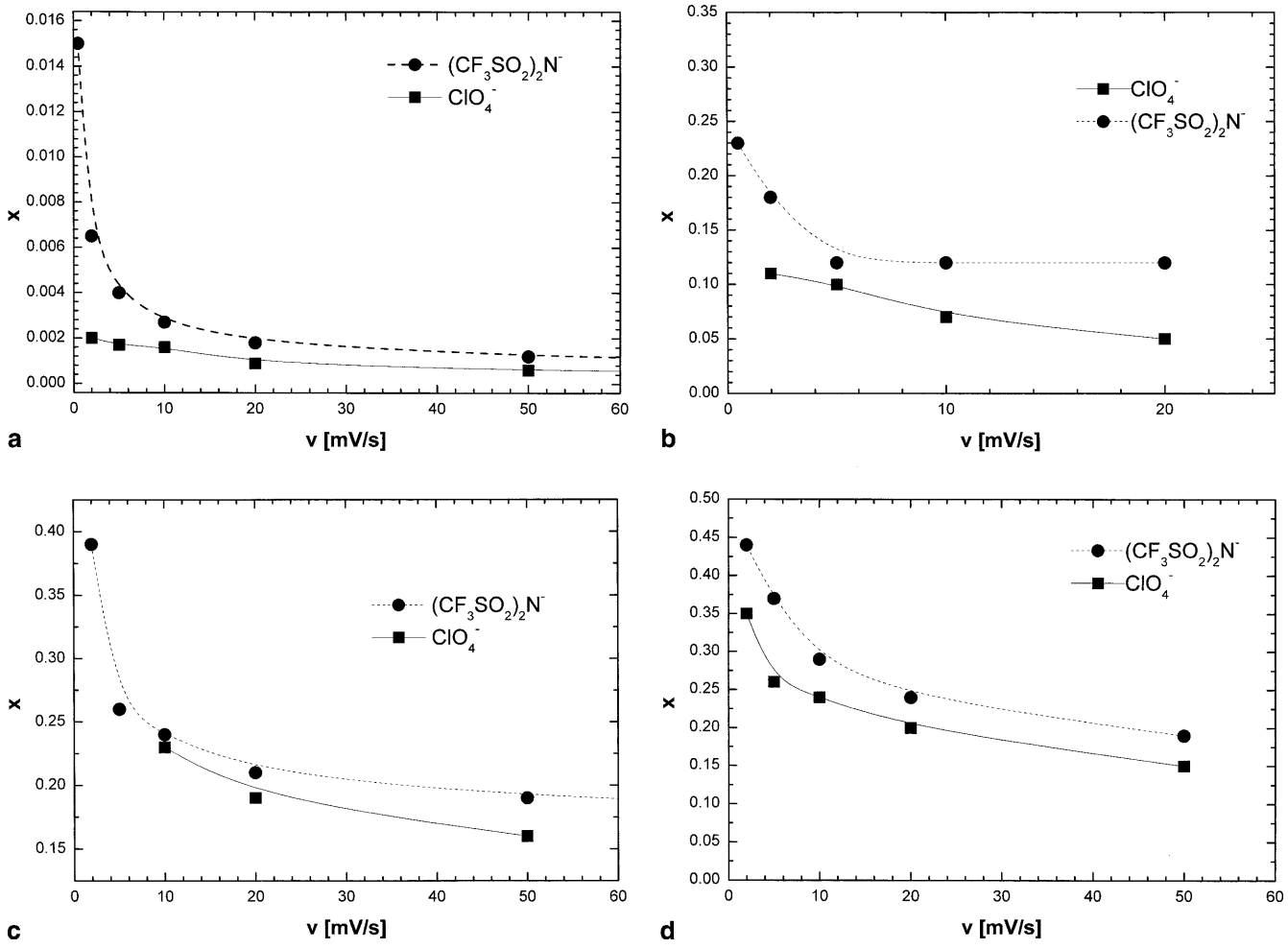

Fig. 5 Dependence of the coefficient x on the scan rate for anatase electrodes with different microstructures: **a** single-crystal, **b** spray pyrolysis, **c** electrodeposited, **d** mesoscopic electrodes in propylene carbonate solutions with different electrolytes

x can be linked to a small electrode area ($\sim$4 mm^2) and to a restricted transport of lithium in the crystal, since the estimated diffusion length of Li in TiO_2 on the time-scale of 1000 s is just $\sim$0.1 μm (assuming the diffusion coefficient 1.6×10^{-13} cm^{-2} s^{-1} [20]).

The characteristic crystal size of the polycrystalline electrodes is comparable or smaller than the Li diffusion length that we anticipate for given time-scales. So the difference in insertion activity is more likely connected with electrochemical side-reactions proceeding at the anatase/electrolyte solution interface. The charge reversibility reflects possible electrochemical side-reactions (see Fig. 6). Reasonable reversibility was observed only on mesoscopic electrodes. All the other polycrystalline electrodes, as well as single-crystal electrodes, show highly irreversible behavior. While for the mesoscopic electrodes the coulombic efficiency did not fall below 0.9, the spray pyrolysis prepared layers exhibit reversibility of about 0.6, and electrodeposited films dropped to values of about 0.3 for the slow scan rates. Similar values to the case of the electrodeposited layers were observed also on single-crystal electrodes. These values indicate that most of the charge during the cathodic scan takes part in parasitic electrochemical side-reactions on spray pyrolysis and electrodeposited electrodes. Charge reversibility was always higher in ClO_4^- containing solutions regardless of the electrode microstructure. This may be attributed to a higher trace water content and in this way to lower redox stability of $N(CF_3SO_2)_2^-$ containing solutions.

Electrode mass behavior

As predicted by Eq. 1, lithium insertion into anatase is connected with increase of electrode mass, and vice versa. A comparison of the net mass changes associated with insertion (reduction) and extraction (oxidation) indicates a total mass irreversibility of the whole electrode process, which may be either of kinetic origin (trapping of Li^+ in the structure) [13] or caused by an irreversible side-reaction. One may distinguish between these processes by comparing coulombic and mass reversibility. While in the case of Li trapping one expects the same values of coulombic and mass reversibility, in

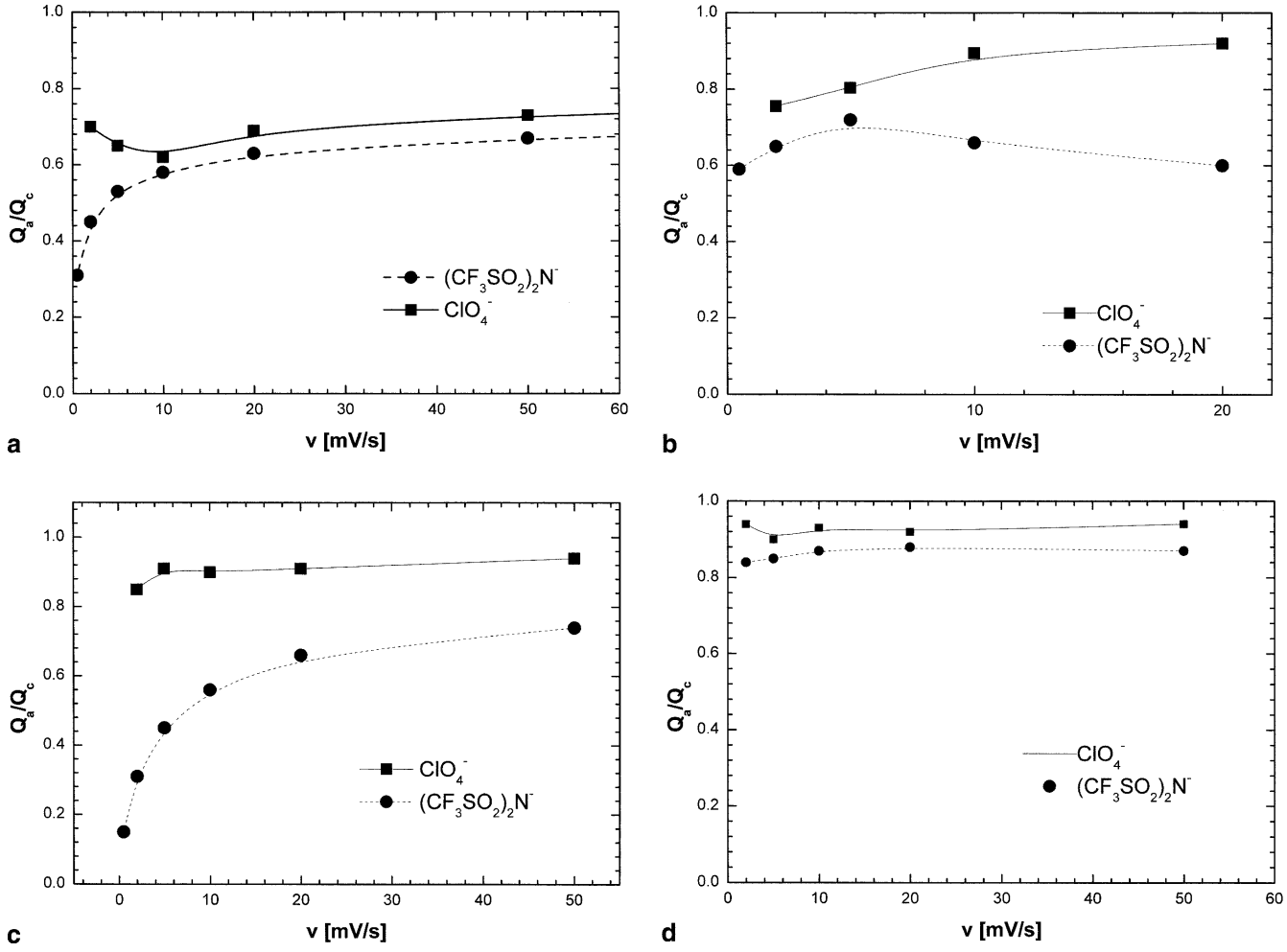

Fig. 6 Charge reversibility Q_a/Q_c as function of scan rate for anatase electrodes with different microstructures: **a** single-crystal, **b** spray pyrolysis, **c** electrodeposited, **d** mesoscopic electrodes in propylene carbonate solutions with different electrolytes

the case of electrochemical side-reactions the coulombic and mass reversibility of a given electrode will vary. It is caused by an electrode mass increase due to formation of carbonate layers [30] during electrochemical side-reactions.

Mass reversibility ($\Delta m_a/\Delta m_c$) as a function of scan rate for different electrodes is shown in Fig. 7a–c. Mesoscopic anatase electrodes show roughly the same values for mass and coulombic reversibility (compare Figs. 6d and 7c), which means that the side reactions proceed only to a small extent. On the other hand, electrodeposited and spray pyrolysis prepared films show a pronounced discrepancy between charge and mass reversibility. The mass reversibilty differs also for perchlorate and $(CF_3SO_2)_2N^-$ containing solutions. The ClO_4^- containing solutions, which exhibit more favorable coulombic reversibility, lag significantly behind $(CF_3SO_2)_2N^-$ containing solutions in mass reversibility. This difference points towards a different course for the electrochemical side-reactions in both electrolytes.

A complementary characterization of electrode mass behavior can be obtained from an apparent molar mass $\delta(\Delta m)/\delta n$, which relates the observed electrode mass change to passed charge according to Eq. 1. Typical Δm vs. Q and $\delta(\Delta m)/\delta n$ vs. n curves for Li^+ insertion/extraction at various scan rates are plotted in Figs. 8 and 9. Assuming the validity of Faraday's law, the theoretical $\delta(\Delta m)/\delta n$ value should be independent of passed charge and equal to 7 g mol^{-1} and –7 g mol^{-1} (molar mass of Li^+) for the insertion and extraction processes, respectively. The response of real systems is, however, generally a function of the passed charge. The deviations from Faraday's law are more evident at high scan rates and in more concentrated electrolyte solutions. While cycling the electrode at a high scan rate (see Fig. 8a) the electrode mass is initially independent of the injected charge, then it starts to decrease with injected charge. After passing through a minimum the electrode mass starts to steeply increase. Expressing the signal in terms of the apparent molar mass the $\delta(\Delta m)/\delta n$ starts at negative values and then significantly increases (see Fig. 9a). The mass change signal from the anodic scan shows a pronounced hysteresis, i.e. the electrode mass still increases although the lithium is, according to charge, already extracted. With decreasing scan rate the

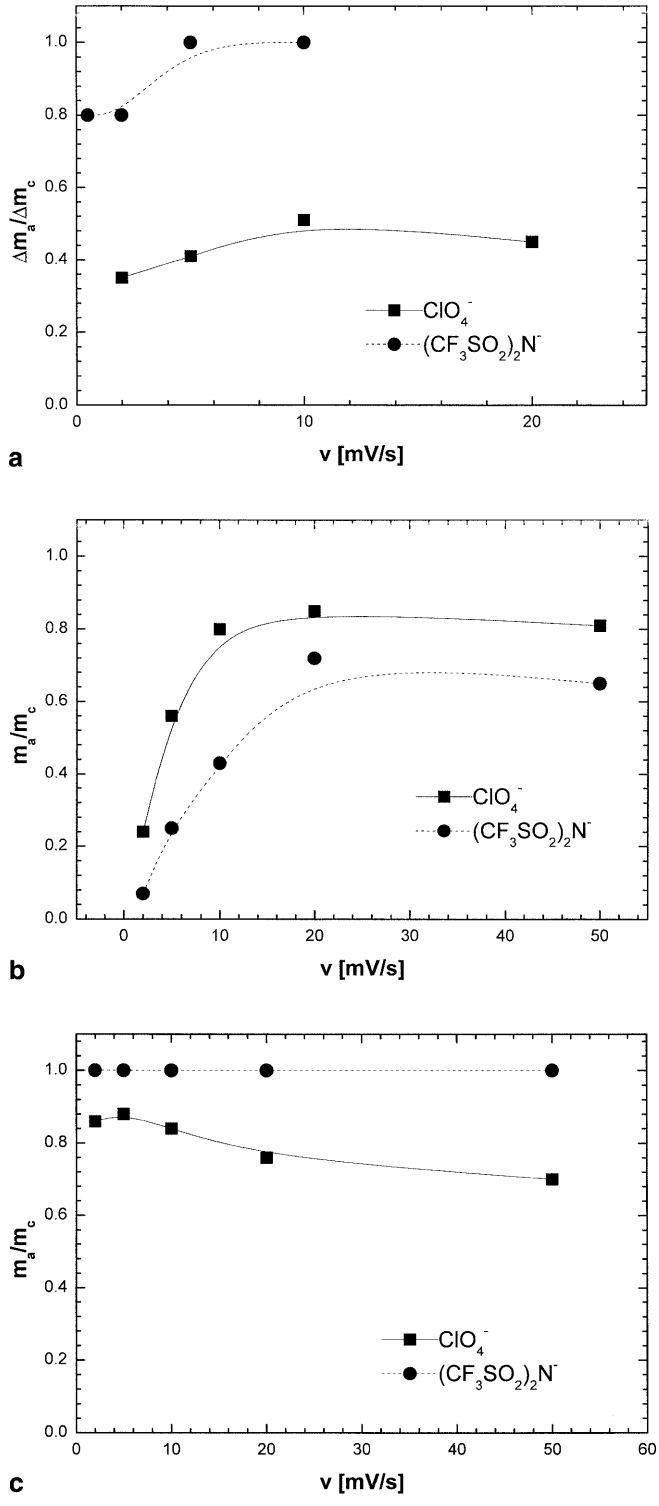

Fig. 7 Mass reversibility $\Delta m_a/\Delta m_c$ as a function of scan rate for electrodes with different microstructures: **a** spray pyrolysis prepared, **b** electrodeposited, **c** mesoscopic electrodes in propylene carbonate solutions with different electrolytes

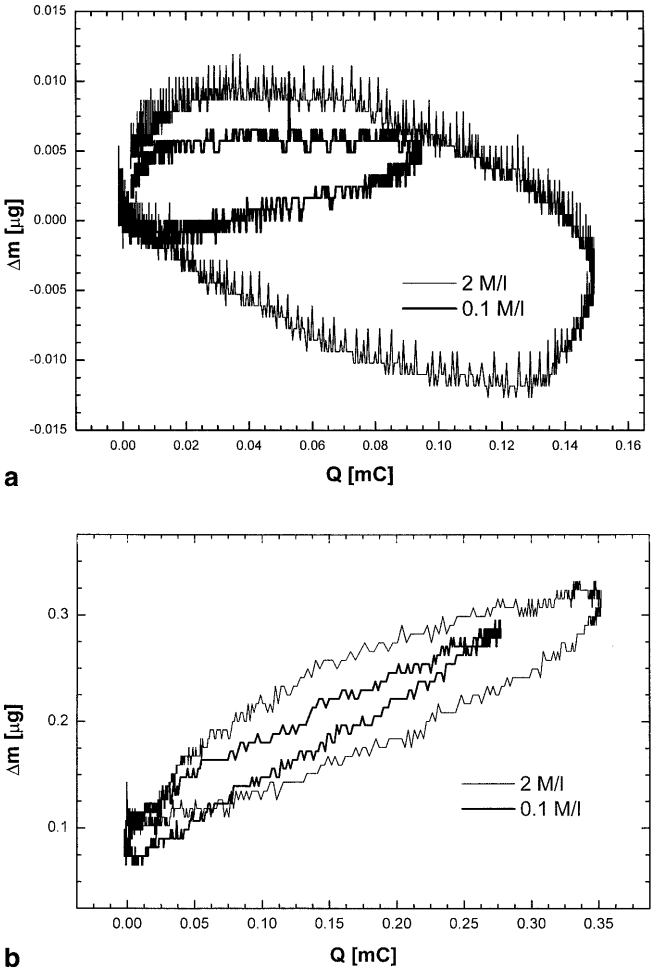

Fig. 8 Typical $\delta(\Delta m)/\delta n$ vs. Q curves for lithium insertion into an anatase mesoscopic electrode during cyclic voltammetry in 0.1 M (*thick line*) and 2.0 M (*thin line*) $Li(CF_3SO_2)_2N$/propylene carbonate solutions at **a** 100 mV s^{-1}, **b** 1 mV s^{-1}

hysteresis decreases. The same effect is also apparent on decreasing the electrolyte concentration (see Fig. 8b). In diluted solutions the hysteresis vanishes at scan rates lower than 1 mV s^{-1} and the apparent molar mass becomes independent of passed charge, equaling 7 and –7 g mol^{-1} for the reduction and oxidation processes, respectively.

Such effects are rather complex and can be understood by taking into account all contributions to the QCM signal. The QCM reading does not reflect the mass fluxes at the electrode/electrolyte interface but it is rather sensitive to mass fluxes at an outer boundary of a thin electrolyte layer, adjacent to the electrode and oscillating together with the electrode [31]. The measured signal therefore does not reflect only Li flux towards or away from the electrode but it involves also contributions of other processes, which can cause mass transport in the electrode vicinity. It may be, for example, solvent or solute transport in the liquid phase triggered by migration [32] or convection [33]. Such contributions are not expressed in Eq. 1.

Since the experiments were performed at unsupported conditions we must take into account that the process of electron injection into TiO_2 causes significant changes of the composition in an electrolyte layer adjacent to the

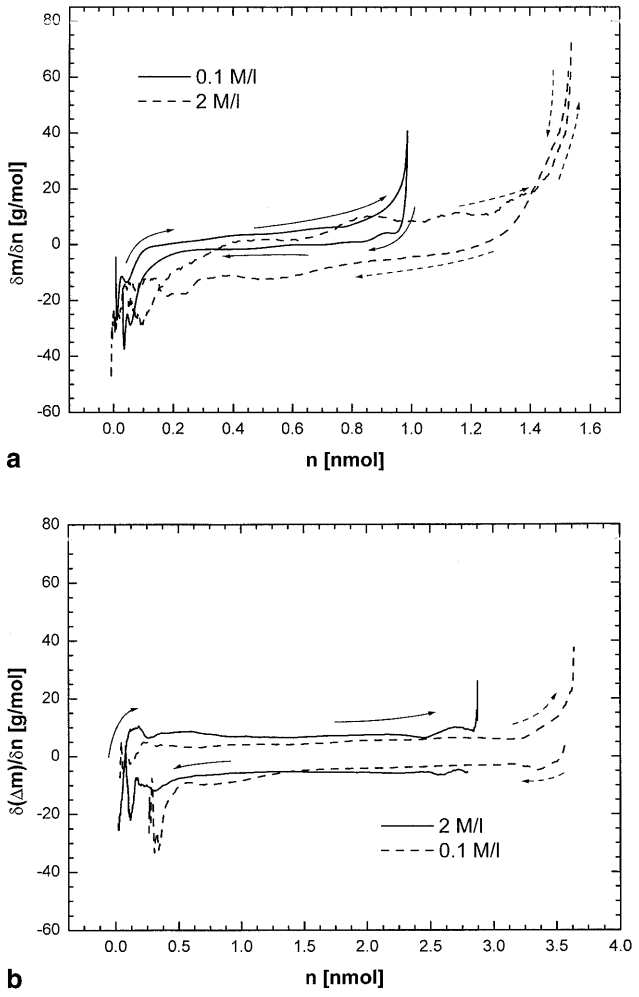

Fig. 9 Typical $\delta(\Delta m)/\delta n$ vs. n curves for lithium insertion into an anatase electrode during cyclic voltammetry in 0.1 M (*solid line*) and 2.0 M (*dashed line*) $Li(CF_3SO_2)_2N$/propylene carbonate solutions at **a** 100 mV s^{-1} and **b** 1 mV s^{-1}

electrode. Electron injection into TiO_2 can be generally compensated by adsorption/insertion of a cation. In both cases there occurs a transport of the anions from the electrode. In the case of adsorption, the anions are transferred to the diffuse part of the double layer; in the case of bulk insertion, we can expect a development of an electrolyte concentration gradient between the electrode surface and the bulk of the electrolyte solution. The initial zero mass change suggests an adsorption compensation of the charge injected into anatase, since the thickness of the electrical double-layer is smaller than that of the electrolyte layer affecting the QCM reading, so there should be no process influencing the QCM reading. Subsequent charge injection compensated by Li insertion into the bulk of the electrode develops concentration gradients of both Li^+ and of the anions into the solution. Mass fluxes of both cations and anions triggered by these gradients (which have an opposite orientation) control therefore the QCM signal. Since the molar mass of the anions is substantially bigger than that of the cations, the total electrode mass signal is negative.

A steep arise of the electrode mass at the end of the cathodic scan, which continues also at the beginning of the anodic scan, and pronounced hysteresis between cathodic and anodic scan data, however, indicate a process which is not governed electrostatically but which involves neutral species [34]. Although neutral species (solvent and ion pairs) cannot enter the material of the electrode, a transfer of these species in the vicinity of the electrode is possible. An electrolyte concentration gradient leads also to the formation of a density gradient. Since the electrode in our experimental arrangement was mounted horizontally at the bottom of the cell, we may expect the electrolyte layer adjacent to the electrode to show a minimum density during lithium insertion (cathodic scan) and a maximum density during lithium extraction (anodic scan). The density gradient developing during insertion then can cause free convection, which may transfer also neutral species (e.g. solvent, ion pairs) which are not involved in the electrode reaction into the volume, affecting the QCM reading. Since the convection is primarily controlled by the density gradient, it will affect the electrode mass signal also at the beginning of the subsequent anodic process. This explains positive values of the apparent molar mass during initial stages of the lithium extraction process as well as hysteresis between anodic and cathodic branches of both Δm vs. Q and $\delta(\Delta m)/\delta n$ vs. n curves. The contribution of the convection to the total QCM reading is more significant at high scan rates, when the gradients develop rather quickly. At slower polarization rates the gradients develop more slowly so the density gradients can be compensated by processes in solution. The fact that the hysteresis between anodic and cathodic branches of the both Δm vs. Q curves is more pronounced in more concentrated solutions also supports this model.

Conclusions

Insertion activity of titanium dioxide (anatase) is strongly affected by differences in electrode morphology. The insertion capacity increases with decreasing crystal size. The values of x observed during cyclic voltammetry, however, did not exceed 0.44. The lowest insertion activity observed on single crystals is probably restricted by limited penetration of the lithium into the crystal. Insertion activity on polycrystalline electrodes is substantially higher. In the case of electrodeposited and spray pyrolysis prepared electrodes, it is restricted by electrochemical side-reactions. A small promotion of the insertion in $(CF_3SO_2)_2N^-$ containing solutions over that in ClO_4^- containing solutions was observed. The origin of this effect remains, however, unclear. Insertion/extraction processes are connected with mass ingress and egress, respectively. $\delta(\Delta m)/\delta n$ values deviate significantly from the value predicted by Faraday's law during the cyclic voltammetry. It can be explained by (1) a transfer of anions in solution from the electrode owing to electroneutrality requirements and by (2) free convection

triggered by density gradients developing during the insertion process.

Acknowledgements This work was supported by the Grant Agency of the Czech Republic under contract no. 203/96/1088 and by the Grant Agency of the Academy of Sciences of the Czech Republic under contract no. A4040804.

References

1. Bonino F, Busani L, Lazzari M, Manstretta M, Rivolta B, Scrosati B (1981) J Power Sources 6:261
2. Ohzuku T, Takehara Z, Yoshizawa S (1979) Electrochim Acta 24:219
3. Macklin WJ, Neat RJ (1992) Solid State Ionics 53–56:694
4. Kanamura K, Yuasa K, Takehara Z (1987) J Power Sources 20:127
5. Ohzuku T, Kodama T, Hirai T (1985) J Power Sources 14:153
6. Huang SY, Kavan L, Grätzel M, Exnar I (1995) J Electrochem Soc 142:142
7. Ohzuku T, Hirai T (1982) Electrochim Acta 27:1263
8. Ottaviani M, Panero S, Morsilli S, Scrosati B (1986) Solid State Ionics 20:197
9. Kavan L, Kratochvilová K, Grätzel M (1995) J Electroanal Chem 394:93
10. Zachau-Christiansen B, West K, Jacobsen T, Atlung S (1988) Solid State Ionics 28–30:1176
11. Zachau-Christiansen B, West K, Jacobsen T, Skaarup S (1992) Solid State Ionics 53–56:364
12. Murphy DW, Cava RJ, Zahurak SM, Santoro A (1983) Solid State Ionics 9–10:413
13. Kavan L, Fattachova D, Krtil P (1999) J Electrochem Soc 146:375
14. Lindström H, Södergen S, Solbrand A, Rensmo H, Hjelm J, Hagfeldt A, Lindquist SE (1997) J Phys Chem B 101:7710
15. Södergen S, Siegbahn H, Rensmo H, Lindström H, Hagfeldt A, Lindquist SE (1997) J Phys Chem B 101:3087
16. Lindström H, Södergen S, Solbrand A, Rensmo H, Hjelm J, Hagfeldt A, Lindquist SE (1998) J Phys Chem B 101:7717
17. Cava RJ, Murphy DW, Zahurak SM, Santoro A, Roth RS (1984) J Solid State Chem 53:64
18. Murphy DW, Greenblatt M, Zahurak SM, Cava RJ, Waszczak JV, Hull GW, Hutton RS (1982) Rev Chim Miner 19:441
19. Cantao MP, Cisneros JI, Torresi RM (1994) J Phys Chem 98:4865
20. Kavan L, Grätzel M, Gilbert SE, Klemenz C, Scheel HJ (1996) J Am Chem Soc 118:6716
21. Kavan L, O'Regan B, Kay A, Grätzel M (1993) J Electroanal Chem 346:291
22. Kavan L, Grätzel M (1995) Electrochim Acta 40:643
23. Kavan L, Grätzel M, Rathousky J, Zukal A (1996) J Electrochem Soc 143:394
24. O'Regan B, Grätzel M (1991) Nature 353:737
25. Nazeeruddin MK, Kay A, Rodicio I, Humphry-Baker R, Mueller E, Liska P, Vlachopolous N, Grätzel M (1993) J Am Chem Soc 115:6382
26. Bruckenstein S, Michalski M, Fensore A, Li Z (1994) Anal Chem 66:1847
27. Ho C, Raistrick ID, Huggins RA, Huggins J (1980) J Electrochem Soc 127:343
28. Webber A (1991) J Electrochem Soc 133:2586
29. Hengerer R, Kavan L, Krtil P, Grätzel M (2000) J Electrochem Soc (in press)
30. Goren E, Chusid O, Aurbach D (1991) J Electrochem Soc 138:L6–L9
31. Buttry DA (1991) In: Bard AJ (ed) Electroanalytical chemistry, vol 17. Dekker, New York, p 1
32. Bohnke O, Vuillemin B, Gabrielli C, Keddam M, Perrot H, Takenouti H, Torresi R (1995) Electrochim Acta 40:2755
33. Krtil P, Nishimura S, Yoshimura M (1999) Electrochim Acta 44:3911
34. Hillman AR, Bruckenstein S (1993) J Chem Soc Faraday Trans 89:399